JACS
JOURNAL OF THE AMERICAN CHEMICAL SOCIETY
pubs.acs.org/JACS
Article

Planar Chiral Metallopolymers for Electrochemically Mediated Enantioselective Separations

Jemin Jeon,[‖] Yuri Giovane Kappenberg,[‖] Ankit Kumar Gautam, Ching-Yu Chen, Johannes Elbert, Alexander V. Mironenko, Fabio Zazyki Galetto,* and Xiao Su*

Cite This: J. Am. Chem. Soc. 2025, 147, 17880−17889
Read Online
ACCESS | Metrics & More | Article Recommendations | Supporting Information

ABSTRACT: The molecular design of redox-responsive interactions can unlock new pathways for enantioselective separations. While chiral redox molecules are powerful platforms for molecular recognition, their implementation in enantioselective separations has remained elusive due to limitations in enantioselectivity and a lack of robust redox electrosorbents. Here, we design a redox-responsive polymer with planar chirality that can achieve exceptional enantioselectivity for the separation of biomolecules. Planar chirality is generated through the insertion of a substituent onto the cyclopentadienyl ring of an oxazoline-conjugated ferrocene with the stereochemical synthesis route guided by the point chirality at the oxazoline moiety. These planar chiral ferrocenes demonstrated significantly stronger enantioselective interactions than the equivalent ferrocenes with only point chirality. Electronic structure calculations revealed the key role of planar chirality, where the inserted functional groups can either coordinatively or antagonistically contribute to complexation, resulting in enhanced enantioselective interactions. Planar chiral metallopolymers were synthesized and evaluated for electrochemical enantioselective adsorption of *N*-Boc−proline, with over 99% enantiomeric excess achievable within seven theoretical stages in a multistage cascade. Planar chirality combined with redox electrochemistry offers a promising path for electrochemically mediated enantioselective separations.

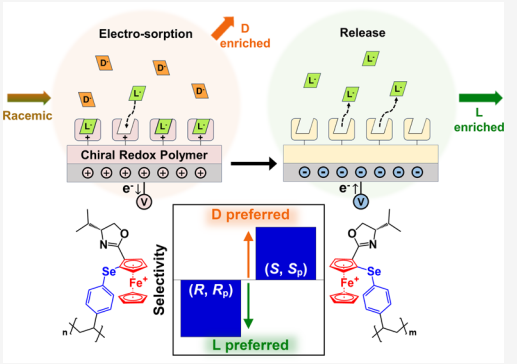

INTRODUCTION

Redox-responsive materials with tunable material properties upon electron transfer have been leveraged for a broad range of applications, including immunotherapy,[1] actuators,[2] ion transport and separation,[3,4] as well as chiral catalysis and sensing.[5−7] Recently, redox-mediated separations have gained significant attention in selective ion separations due to the control of specific interactions and enhanced adsorption capacity.[3] In parallel, chiral redox molecules have provided versatile platforms for enantioselective recognition.[8,9] However, the successful deployment of redox-responsive materials for chiral separations has been elusive due to limitations in enantioselectivity and synthesis hurdles to create efficient building blocks for the chiral selectors. In the current work, we impart planar chirality onto a ferrocene-based metallopolymer to enhance enantioselective interactions and enable the electrochemical purification of enantiomers.

Metallopolymers are promising platforms due to their synthetic versatility and redox activity. Ferrocene (Fc)-based polymers enable reversible ion sorption,[10] where the electrochemical oxidation of Fc to ferrocenium (Fc^+) drives anion binding.[11−14] Furthermore, metallocene building blocks allow for the modular insertion of planar chirality by synthetic routes.[15] Planar chirality strains the molecular conformation, inducing a strong steric effect[15] which can enhance the overall chirality of a molecule and lead to highly regioselective biological and catalytic activity.[16,17] Thus, planar chiral ferrocenes are promising building blocks for redox polymers that enable enantioselective separations. Despite their intriguing properties, planar chiral ferrocenes have been studied mainly as a chiral precursor or catalyst in the homogeneous phase[18] with no application in electrochemical separations.

Chiral separation is central to the pharmaceutical and biotechnology industries. Over 50% of the new FDA-approved molecules are chiral, and 90% of them are enantiopure.[19,20] Chiral chromatography has been extensively studied with an emphasis on the material development of synthetic and natural chiral stationary phases.[21] However, these chromatographic processes can be intrinsically slow and chemically demanding.[22] For example, the environmental factor (*E* factor; a waste-to-product ratio) of the pharmaceutical industry is among the

Received: February 5, 2025
Revised: April 25, 2025
Accepted: April 28, 2025
Published: May 13, 2025

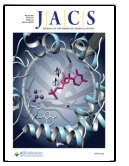

https://doi.org/10.1021/jacs.5c01571
J. Am. Chem. Soc. 2025, 147, 17880−17889

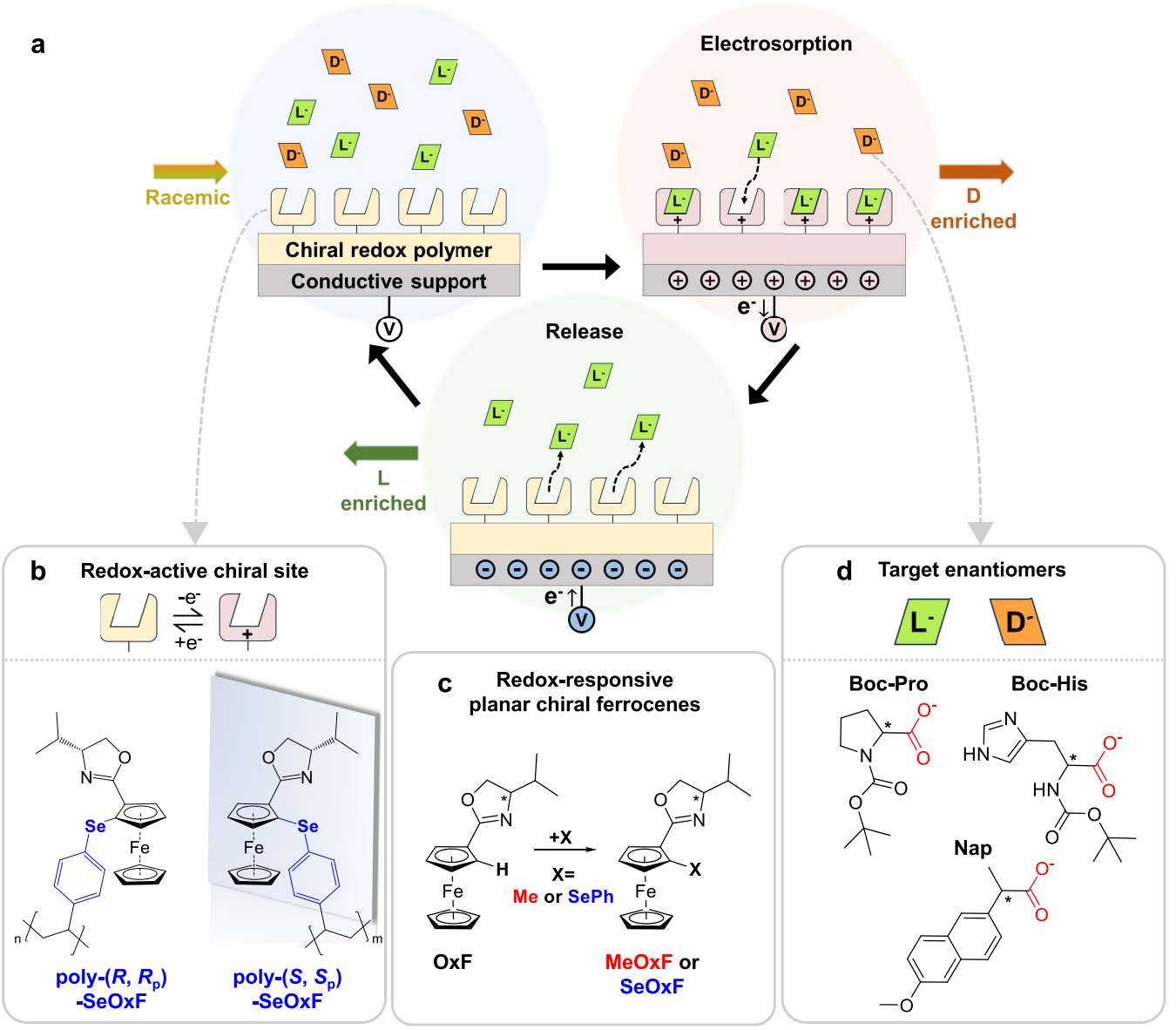

Figure 1. (a) Scheme of the proposed redox-mediated enantioselective separations. Clockwise from the top-left circle: introduction of a racemic mixture in contact with the chiral electrosorbent, then enantioselective binding driven by the oxidation potential, followed by release of adsorbed L enantiomers under a reduction potential. (b) Structure of the chiral metallopolymers evaluated for enantioselective electrosorption in the current work. (c) Design strategy for imparting planar chirality onto the ferrocene redox selectors. $-CH_3$ or $-SePh$ moiety is inserted in an ortho position to chiral-2-oxazoline on the cyclopentadienyl ring of the ferrocene. (d) Target chiral molecules evaluated in this work for molecular recognition and enantioselective separations.

highest in chemical manufacturing,[23] with chromatographic separation being one of the largest contributors to waste generation.[24] Thus, pathways for reducing waste and improving efficiency are needed in enantioselective separations.

Redox-responsive materials are an emerging platform for providing environmentally benign and efficient separation processes for a variety of target molecules, including organic anions,[10] transition metals,[11,13,25] homogeneous catalysts,[12,26] and organohalides.[10,27] Electrochemical control of adsorption can minimize the chemical input and waste generation. However, redox-responsive chiral interfaces to date have been limited to sensing and molecular recognition.[28,29] Thus, redox-responsive heterogeneous interfaces with sufficient chirality and binding reversibility can be powerful platforms for enantioselective separations.

In this work, we pursue a bottom-up design for the chiral redox-responsive macromolecules by creating planar chiral ferrocene building blocks that enable unique enantioselectivity. Our synthetic strategy utilizes chiral-2-oxazolines as the directing group for *ortho*-lithiation in ferrocene, with the careful choice of the inserted group being a fundamental step for the design of successful chiral selectors. Homogeneous molecular recognition measurements reveal that the planar chiral ferrocenes interact with target carboxylates with a higher degree of enantioselectivity than ferrocenes possessing only point chirality. The planar chiral building blocks are then incorporated into a redox metallopolymer, which is used as an electrosorbent matrix. The functionalized electrodes with a

https://doi.org/10.1021/jacs.5c01571
J. Am. Chem. Soc. 2025, 147, 17880−17889

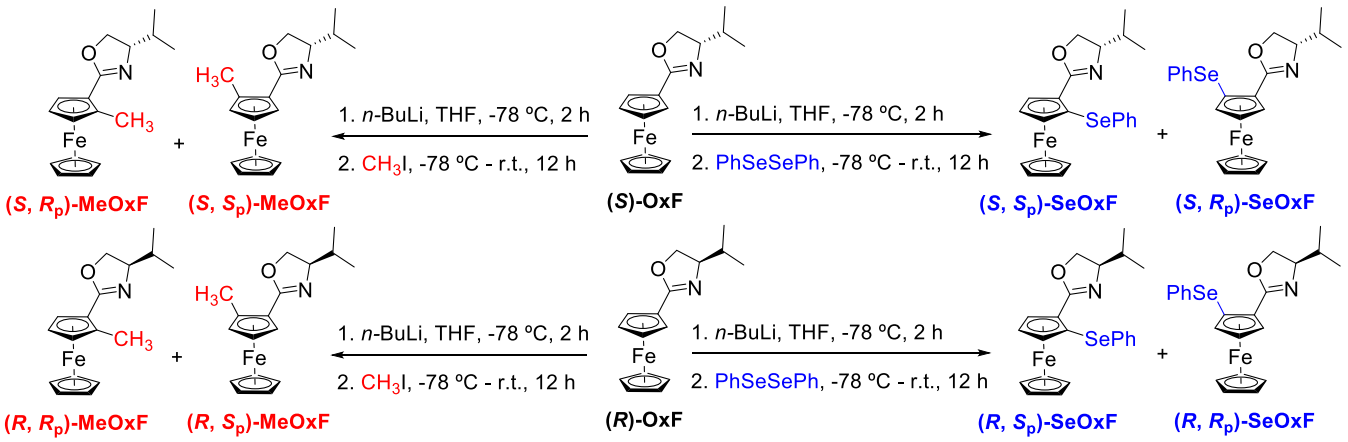

Figure 2. Synthesis of the four stereoisomers for each of the planar chiral redox selectors, MeOxF and SeOxF, via a 2-oxazoline ring-directed *ortho*-lithiation strategy.

chiral redox polymer achieve the enantioselective separation of amino acids through potential-assisted electrosorption and release (Figure 1a). Density functional theory (DFT) calculations reveal that noncovalent interactions of the functional groups forming the planar chirality play either a coordinative or antagonistic role toward the largely electrostatics-driven Fc^+ and carboxylate (COO^-) interaction with the target enantiomers, leading to the high enantioselectivity of the planar chiral ferrocenes. A counter-current multistage design using seven theoretical stages can achieve >99% enantiomeric excess (%ee) for *N*-Boc−L−proline, demonstrating the applicability of these electrochemical platforms for enantioselective purification.

RESULTS AND DISCUSSION

Design and Selection of Planar Chiral Platforms for Enantioselective Interactions. Figure 1c shows the molecular design of the planar chiral ferrocene selectors studied in this work. Ferrocenes with two different functional groups in adjacent positions on the cyclopentadienyl ring have planar chirality. The molecular stiffness of ferrocene makes it an ideal building block for creating chiral macromolecules, as steric hindrance can facilitate the noncovalent interactions of target molecules with the functional groups adjacent to ferrocene. These effects can lead to stronger enantioselective recognition and even macromolecular chirality in certain cases.[30−32]

For the design of the chiral building blocks, a 2-oxazoline moiety was chosen due to its point chirality, which can act as the directing group to control the stereoselective *ortho*-lithiation step for the introduction of planar chirality into ferrocene. The functional groups selected for insertion onto the cyclopentadienyl ring were methyl ($-CH_3$) and selenium phenyl (−SePh). Methyl was chosen as a relatively non-polarizable, small alkyl group to serve as a control for probing the effect of planar chirality against point chirality in its simplest form. The insertion of the selenium phenyl group, on the other hand, introduces a more disruptive group that can have potential charge-transfer interactions as well as greater steric hindrance than the methyl group. The phenyl group can also provide a platform for CH···π or π···π interaction. Planar chiral polymers based on these design principles were synthesized either by radical polymerization of chiral ferrocene monomers (poly(R, R_p) or (S, S_p)−SeOxF) or by functionalization of a polymer with a chiral ferrocene monomer (poly(S, R_p) −MeOxF) to be used as a redox-switchable electrosorbent in enantioselective separation (Figures 1b,4).

N-Boc−amino acids (such as *N*-(*tert*-butoxycarbonyl)−proline (Boc−Pro) and *N*-(*tert*-butoxycarbonyl)−histidine (Boc−His) and Naproxen (Nap) in carboxylate form (Figure 1d)) were chosen as model target chiral molecules owing to their anionic nature and importance as precursors for active pharmaceutical ingredients (APIs).[33] In our previous study on molecular recognition, redox selectors possessing point chirality had no selectivity toward Boc−Pro and naproxen enantiomers in nonaqueous media despite possessing a strong HB acceptor group (e.g., amide and amine).[34]

Here, we envision that the insertion of the planar chirality can enhance the enantioselectivity of a chiral ferrocene between target enantiomers beyond point chirality.

Synthesis and Characterization of Planar Chiral Redox Molecules, Monomers, and Polymers. The (S_p) and (R_p) diastereomeric pairs of two planar chiral redox ferrocenes (MeOxF and SeOxF) were synthesized via *non*-selective *ortho*-lithiation[35] using chiral-2-oxazolines and a reaction with MeI or PhSeSePh as an electrophile, followed by chromatographic separation of the diastereomers. The enantioselective recognition of each of the stereoisomers toward the target chiral molecules was investigated to select the most optimal systems for demonstrating enantioselective separations (Figure 2 and Supporting Information for synthesis details). The nomenclature rule proposed by Schlögl is used in this work to define the absolute configuration of planar chiral ferrocene compounds.[36]

The optical property of the planar chiral redox selectors was investigated using optical rotatory dispersion (ORD) and circular dichroism (CD). The stereoisomers of both MeOxF and SeOxF showed absolute values of the specific rotation (between −459 and 440°) higher than those of (*S*)- and (*R*)-3 (−111 and 108°, respectively) (Table S1). Solution CD of the stereoisomers of OxF, MeOxF, and SeOxF in acetonitrile (MeCN) further confirmed their relative chirality (Figure 3a,b). The Cotton effect observed near 520 nm of the peak wavelength with all stereoisomers was attributed to the d-d electron transition of the iron in the ferrocene unit, ultraviolet (UV)−vis spectra in Figure S52. Overall, ORD and CD measurements showed that the addition of the planar chirality with a methyl or selenium phenyl group enhanced the optical properties of the stereoisomers compared to (*S*) and (*R*)−

https://doi.org/10.1021/jacs.5c01571
J. Am. Chem. Soc. 2025, 147, 17880−17889

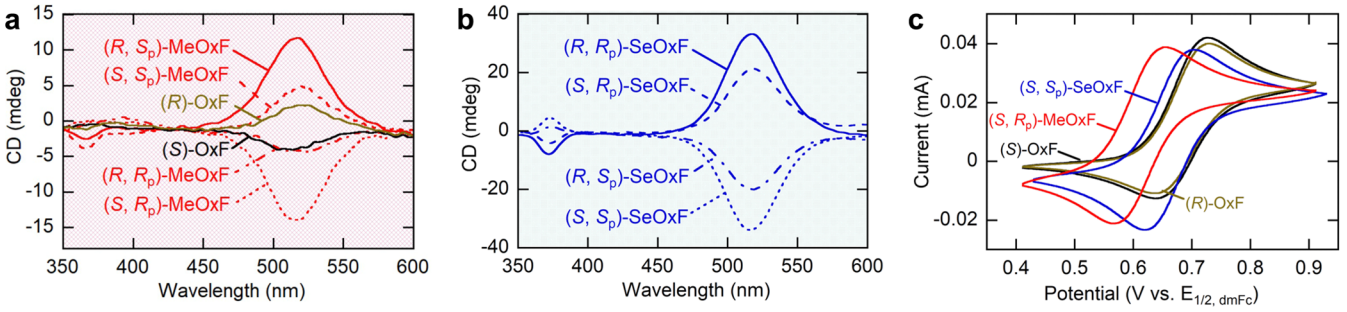

Figure 3. CD and CV of planar chiral redox selectors. (a, b) Circular dichroism of 10 mM OxF enantiomers, MeOxF diastereomers (a), and SeOxF diastereomers (b) in MeCN. (c) Cyclic voltammetry of 1 mM (*S*)−OxF (black), (*R*)−OxF (brown), (*S*, R_p)−MeOxF (red), and (*S*, S_p)−SeOxF (blue) in 0.1 M $TBAPF_6$ MeCN.

OxF. In cyclic voltammetry (CV) measurement, the half potentials ($E_{1/2}$) of the stereoisomers were similar to each other within 5 mV (Figures 3c and S53). (*S*)−OxF had the highest half potential ($E_{1/2}$) (682 mV vs decamethylferrocene (dmFc)), followed by (*S*, S_p)−SeOxF (662 mV vs dmFc) and (*S*, R_p)−MeOxF (608 mV vs dmFc) owing to the electron-donating groups −SePh[37] and $-CH_3$,[38] respectively (Table S2).

For the synthesis of the chiral redox polymers, the corresponding monomers were prepared by a diastereoselective strategy using the chiral-2-oxazoline ring as an inducer for asymmetry[35] (see Figure 4 and Supporting Information for synthesis details). A polymer functionalization by the thiol−ene reaction was used for poly−MeOxF, and a radical polymerization with azobis(isobutyronitrile) (AIBN) was used to create the final poly−SeOxF redox polymers. (*R*, R_p)−/(*S*, S_p)−SeOxF and (*S*, R_p)−MeOxF were selected due to their higher enantioselectivity toward Boc−Pro and Boc−His enantiomers, respectively (Figure 6a,b). The solution CD (Figure S65) showed that the small molecule, monomeric, and polymeric forms of each (*R*, R_p) and (*S*, S_p)−SeOxF are similar in CD intensity, with the opposite Cotton effect between the enantiomers. Compared to their corresponding polymers, the solid CD spectra of the monomers, mono-SeOxF and mono-MeOxF, had a blue-shifted Cotton effect in the π-π^* electron transition region due to the longer conjugation with the vinyl group than their polymers (Figures S66, S67). Two-dimensional (2D) NOESY found intramolecular interactions of the isopropyl group with the phenyl and backbone of the polymer (Figure S68), and the redox activity of the ferrocene unit in the polymers was confirmed by CV (Figure S70 and Table S4).

Redox-Mediated Enantioselective Recognition by Planar Chiral Ferrocenes. Half potential shift ($\Delta E_{1/2}$) of the planar chiral ferrocenes was utilized to probe a binding strength between a chiral ferrocene and a target molecule in a homogeneous solution, following methods established in the literature.[34,39] The half potential shift difference ($\Delta\Delta E_{1/2} = \Delta E_{1/2,\ L\ \text{or}\ (S)} - \Delta E_{1/2,\ D\ \text{or}\ (R)}$) was calculated to compare the enantioselectivity of the chiral ferrocenes toward the target molecules (Figure S56). The $\Delta\Delta E_{1/2}$ results show that the planar chiral selectors generally had higher enantioselectivity than the point chiral selectors in nonaqueous aprotic media (Figure 5). (*S*, R_p)−MeOxF and (*S*, S_p)−SeOxF were picked for further enantioselectivity comparison due to their same planar chirality with respect to the oxazoline ring. (*S*)−OxF, which contains the same point chirality with (*S*, R_p)−MeOxF and (*S*, S_p)−SeOxF, was also tested. With Boc−Pro enantiomers, (*S*, S_p)−SeOxF showed significantly higher $|\Delta\Delta E_{1/2}|$ (27.9 mV) than (*S*, R_p)−MeOxF (9.15 mV) and (*S*)−OxF (1.70 mV). With Nap and Boc−His, (*S*, R_p)−MeOxF had the highest $|\Delta\Delta E_{1/2}|$ (15.0 mV for Nap and 8.22 mV for Boc−His). In addition, the point chiral selectors from our previous work,[34] *N*-(1-ferrocenylethyl) methacrylamide and 2-((1-ferrocenylethyl)(methyl)amino) ethyl methacrylate, showed little to no enantioselectivity ($|\Delta\Delta E_{1/2}|$=0.40−3.08 mV) for Boc−Pro, Nap, and Boc−His (molecular structures and $|\Delta\Delta E_{1/2}|$ reported in Figure S54). The molecular recognition comparison among the OxF derivatives and the point chiral ferrocenes from the previous work[34] demonstrates that planar chirality, even with the simple methyl group, can enhance the enantioselectivity of a chiral redox selector. Furthermore, the judicious target-specific selection of a functional group for the planar chirality (e.g., $-CH_3$ for Nap and Boc−His and −SePh for Boc−Pro) plays an essential role in the enantioselectivity.

Next, the enantioselective recognition of the stereoisomers of OxF, MeOxF, and SeOxF was compared to study the coordinative effect between the point and planar chirality (Figure 6a,b). Boc−His and Boc−Pro were selected as the targets because (*S*, R_p)−MeOxF and (*S*, S_p)−SeOxF showed the highest $|\Delta\Delta E_{1/2}|$ with them in the selectivity screening in MeCN. Methanol (1−5% v/v), a protic solvent, was added into the solution matrix because a decrease in the redox peak of the OxF derivatives over the square wave voltammetry (SWV) cycles was observed due to the irreversible oxidation of the target molecules, and after the addition, the oxidation of the targets was either absent or far away from the oxidation of the OxF derivatives except for Nap (Figure S55). Water was not considered an additive because methanol, a weaker protic solvent, already decreased the enantioselectivity of SeOxF (Figure S57).

The enantiomeric pair (*R*, R_p)−SeOxF and (*S*, S_p)−SeOxF had the highest $|\Delta\Delta E_{1/2}|$ (5.29 and 4.91 mV) with the opposite preference to the Boc−Pro enantiomers —(*R*, R_p)−SeOxF had a bigger negative potential shift with L−Boc−Pro ($\Delta\Delta E_{1/2}$ < 0) and (*S*, S_p)−SeOxF with D−Boc−Pro ($\Delta\Delta E_{1/2}$ > 0) (Figures 6a and S59). The other enantiomeric pair, (*R*, S_p)−SeOxF and (*S*, R_p)−SeOxF, had 2−6.5 times lower $|\Delta\Delta E_{1/2}|$ (0.81 and 2.43 mV) in the similar range with those of OxF and MeOxF stereoisomers (0.50−2.80 mV), suggesting that the (*S*) and (S_p) chirality in SeOxF (or (*R*) and (R_p)) led to a synergistic effect on the enantioselective recognition toward Boc−Pro enantiomers. For Boc−His, (*S*, R_p)−MeOxF showed the highest $|\Delta\Delta E_{1/2}|$ (15.40 mV) with a preference toward Boc−D−His (Figure 6b). Its enantiomer (*R*, S_p)-MeOxF showed a preference toward Boc−L−His ($\Delta\Delta E_{1/2}$ = −9.69

https://doi.org/10.1021/jacs.5c01571
J. Am. Chem. Soc. 2025, 147, 17880−17889

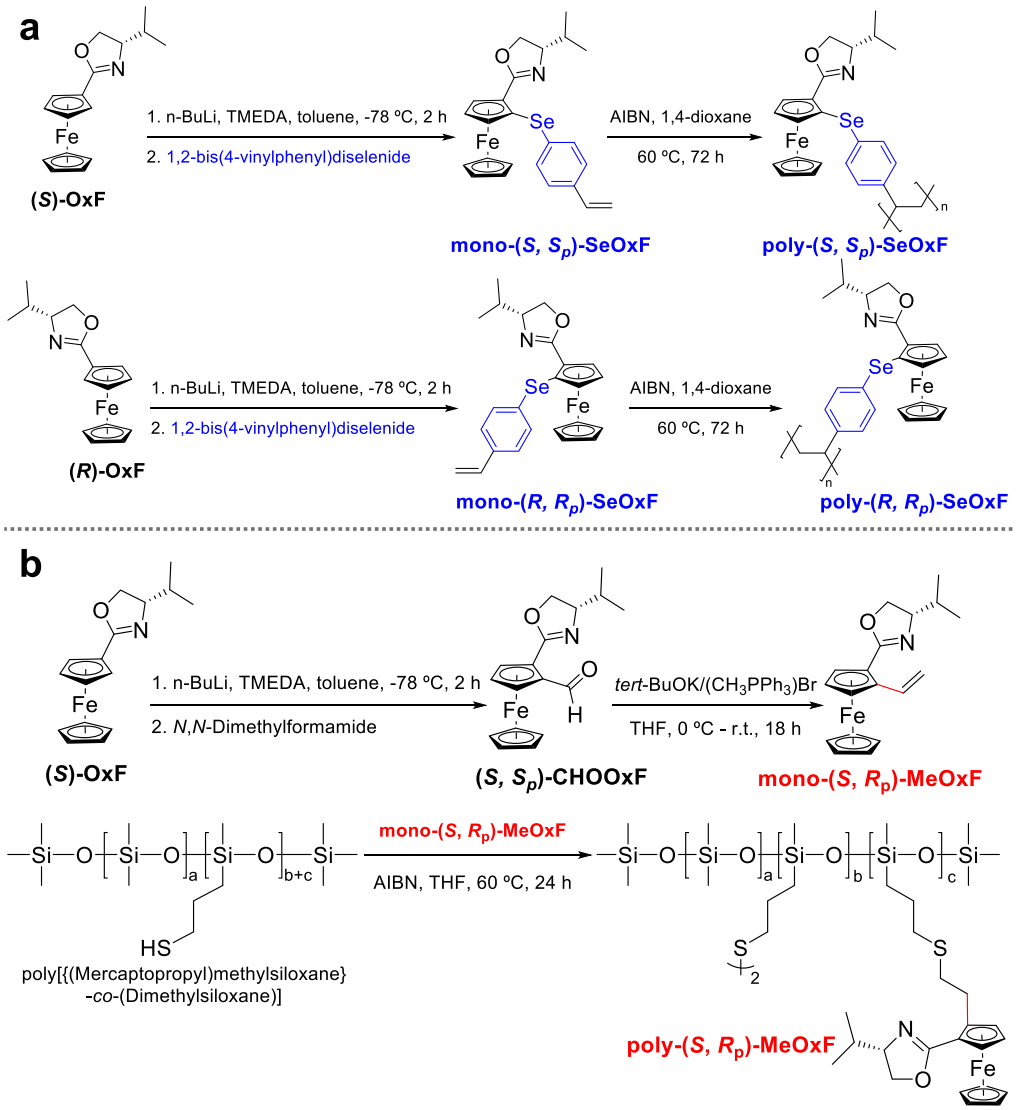

Figure 4. Synthesis of planar chiral redox metallopolymers. (a) Two-step synthetic route used in the syntheses of the poly(S,S_p)−SeOxF and poly(R,R_p)−SeOxF isomers. (b) Three-step synthetic route used in the synthesis of the poly(S,R_p)−MeOxF. In both pathways, the respective monomers were prepared through the diastereoselective *ortho*-lithiation strategy, followed by a radical polymerization step.

mV), confirming the chirality-induced enantioselective recognition. The other enantiomeric pairs, (S, S_p)−MeOxF and (R, R_p)−MeOxF, also had similar $|\Delta\Delta E_{1/2}|$ (8.98 and 9.95 mV) as well as the same target preference with their point chirality counterparts ((S, R_p) and (R, S_p), respectively), implying that the point chirality in MeOxF determined the preference toward Boc−His enantiomers. OxF and SeOxF stereoisomers showed marginal enantioselectivity toward Boc−His (Figures 6b and S60).

The free energy change of the binding (ΔG) between a chiral selector and a target enantiomer was calculated from empirical binding constants to investigate the selectivity of binding through the difference in binding energy change ($\Delta\Delta G = \Delta G_L - \Delta G_D$). An isotherm obtained from the voltametric response against different concentrations of the target enantiomer by titration was used to track the gradual cathodic voltametric shift of a selector. Equilibrium binding constants K^+ and K were obtained by fitting the potential shift over the titration[39] (Figure S63 and Table S3). ΔG of (S, S_p)−SeOxF with Boc−D−Pro (−16.0 kJ/mol) was 1.5 kJ/mol stronger than that with Boc−L−Pro (−14.5 kJ/mol). The opposite was observed with (R, R_p)−SeOxF, for which ΔG with Boc−L−Pro (−16.3 kJ/mol) was 2.1 kJ/mol larger than that with Boc−D−Pro (−14.2 kJ/mol). These $\Delta\Delta G$ of 1.5−2.1

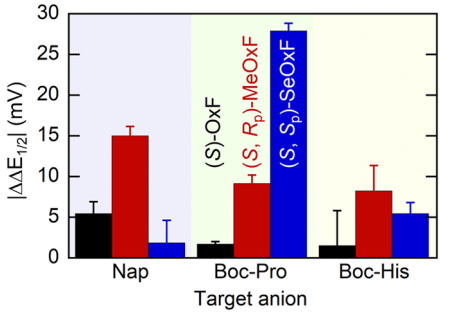

Figure 5. Comparison of the enantioselective recognition between a point chiral ferrocene, (S)−OxF (black), and the planar chiral ferrocenes (S, R_p)−MeOxF (red) and (S, S_p)−SeOxF (blue) based on half potential shift differences ($\Delta\Delta E_{1/2}$) with Nap, Boc−Pro, and Boc−His enantiomers in anhydrous MeCN.

https://doi.org/10.1021/jacs.5c01571
J. Am. Chem. Soc. 2025, 147, 17880−17889

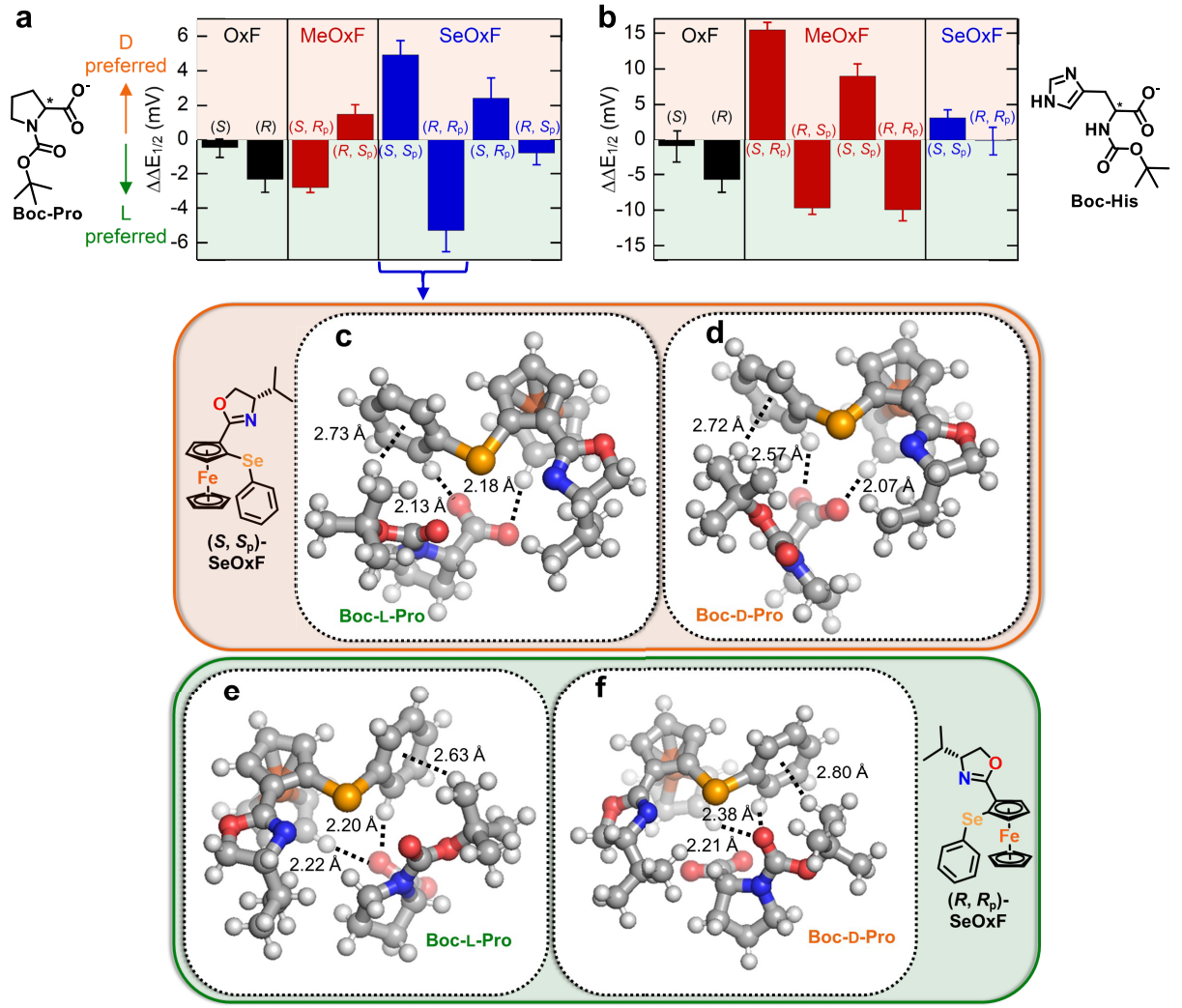

Figure 6. Enantioselective recognition of chiral ferrocene stereoisomers and DFT-optimized structures of the most stable binding geometry. (a, b) Half potential shift difference ($\Delta\Delta E_{1/2}$) of chiral redox ferrocenes with Boc−Pro enantiomers in MeCN (2% MeOH v/v) (a) and Boc−His enantiomers in MeCN (5% MeOH v/v). (c−f) Optimized binding geometry of (S, S_p)−SeOxF with Boc−L−Pro (c) or Boc−D−Pro (d) and (R, R_p)−SeOxF with Boc−L−Pro (e) or Boc−D−Pro (f). C−H···O contacts under 2.6 Å and C−H···π interaction under 3 Å are marked using a dotted line. Orange, yellow, gray, red, blue, and white balls represent Fe, Se, C, O, N, and H atoms, respectively.

kJ/mol are in the same order of magnitude with $\pi-\pi$, dipole−dipole, and weak hydrogen bonding[40] and far above 0.46 kJ/mol of minimum $\Delta\Delta G$ required for base separation in chromatography.[41] Overall, the results from the enantioselective recognition measurements for the planar chiral selectors prove that the enantioselectivity can be dramatically increased simply by inserting planar chirality at the redox unit.

Molecular Mechanism for Enantioselectivity in Planar Chiral Ferrocenes. Electronic structure calculations were carried out to probe the underlying mechanisms of enantioselective binding between the target enantiomers and chiral selectors. First, a geometry optimization using DFT was carried out for pairs between positively charged planar chiral ferrocenes ((S, S_p)−SeOxF, (R, R_p)−SeOxF, (S, R_p)−MeOxF, and (R, S_p)−MeOxF) and anionic target enantiomers (Boc−Pro and Boc−His) to identify their binding configurations exhibiting enantioselectivity (Supporting Information for the DFT method). Due to many possible interaction points, the atomic charges on the (R, R_p)−SeOxF cation were first analyzed, revealing positively charged terminal hydrogens and Se (Figures S83, S84). These hydrogens were expected to interact with the negatively charged oxygens of the target carboxylates. Our hypothesis of [CH···O] interactions was confirmed for a simpler model system using (R)−OxF and formate ($HCOO^-$) (Table S6). The formate result not only brings insights into the binding motifs but also highlights how the implicit solvation during geometry optimization resulted in fewer points of contact and, on average, larger [CH···O] bond lengths. Furthermore, the configurations with formate closer to the functional groups were found to be thermodynamically more stable than those far away. This observation hinted toward the possibility of a favorable binding pocket formed close to the planar chiral center.

We investigated binding for the complexes between (R, R_p) or (S, S_p)−SeOxF and Boc−Pro enantiomer and complexes between (S, R_p)−MeOxF and Boc−His enantiomer due to their high experimental $\Delta\Delta E_{1/2}$ (Figure 6a,b). Learning from the formate system, we generated initial guesses in the binding pocket with several [CH···O] contacts (Table S7). Among all of the binding configurations, the most stable complexes always had carboxylate oxygens of the target molecule close to the C−H termination of the cyclopentadiene ring of Fc^+ of the

https://doi.org/10.1021/jacs.5c01571
J. Am. Chem. Soc. 2025, 147, 17880−17889

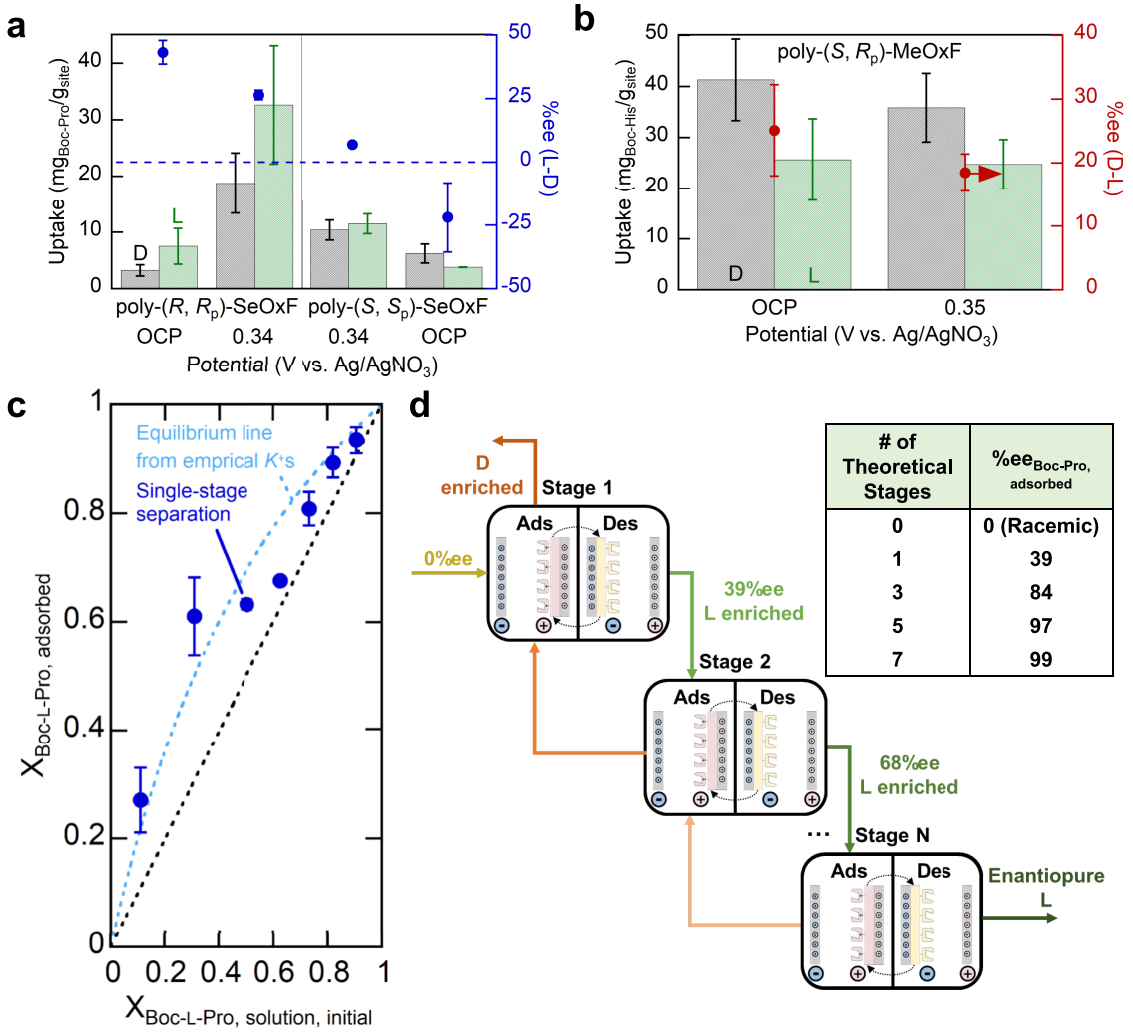

Figure 7. Enantioselective separation using the planar chiral redox polymers. (a) Uptake and enantiomeric excess of Boc−Pro enantiomers adsorbed by poly(S, S_p) or (R, R_p)−SeOxF under 0.34 V of oxidation potential or OCP in MeCN (2% MeOH v/v). (b) Uptake and enantiomeric excess of Boc−His enantiomers adsorbed by poly(S, R_p)−MeOxF under 0.35 V of oxidation potential or OCP in MeCN (5% MeOH v/v). (c) Equilibrium line for electrochemically assisted separation of Boc−Pro enantiomers drawn from empirical K's of (R, R_p)−SeOxF (dotted light blue) and experimentally obtained fraction of adsorbed Boc−L−Pro from the Boc−Pro mixture of different enantiomeric excesses (blue dots). 0.5 mM enantiomer mixture and 20 mM $TBAPF_6$ were used for all separation experiments. (d) Multistage counter-current cascade of the electrochemical separation process, with %ee of L enantiomer listed against the number of theoretical stages. Ads and Des represent adsorption and desorption.

planar chiral ferrocenes. Typical [CH···O] bond lengths in the complexes varied between 2.07 and 2.22 Å (Figures 6c−f and S86, S87), suggesting a predominant electrostatics-driven complexation. The proximity of several oppositely charged atoms ($O^{\delta-}$ with $H^{\delta+}$) allows further stabilization. The phenyl group of SeOxF also enables an additional [CH···π] interaction with the isobutyl group of Boc−Pro enantiomers with bond distances between 2.63 and 2.80 Å (Figure 6c−f), further stabilizing the complexes. Interestingly, the binding geometry of SeOxF with the preferred enantiomer had shorter distances of [COO^-···Fc^+] and [CH···π] than those with the other enantiomer. The enantiomeric pair of the complexes between SeOxF diastereomers and Boc−Pro enantiomers showed mirror-imaged geometries, affirming the correctness of the geometries obtained. The predicted $\Delta\Delta G$ (Figure S85) confirmed the enantioselective binding affinity of (R, R_p) or (S, S_p)−SeOxF toward one Boc−Pro enantiomer over the other, in agreement with the empirically observed binding preference (Table S3). Both the predicted and empirical $\Delta\Delta G$ of (S, S_p)−SeOxF were 1.5 kJ/mol (Boc−D−Pro favored), while the predicted $\Delta\Delta G$ of (R, R_p)−SeOxF was −3.5 kJ/mol (Boc−L−Pro favored), higher than the empirical value of −2.1 kJ/mol.

The structures determining the enantioselectivity of (S, R_p)−MeOxF toward Boc−His enantiomers showed [CH···O] interactions as well. Interestingly, the complex between (S, R_p)−MeOxF and Boc−L−His had two points of interaction (Figure S86): an interaction between one H of the cyclopentadiene ring and COO^- of Boc−L−His and an interaction between the methyl group composing the planar chirality and COO^-. On the other hand, Boc−D−His had a single-point electrostatic interaction with (S, R_p)−MeOxF (Figure S86b). The single-point interaction of Boc−D−His showed more stable complexation than the two-point interaction of Boc−L−His with an energetic difference of 1.4 kJ/mol (Table S8). This selectivity mechanism suggested that the additional interaction was rather antagonistic toward the interaction between the proton of the cyclopentadiene ring and COO^- owing to an unfavorable out-of-plane rotation. The complex between (S, R_p)−MeOxF and Boc−L−His clearly had

https://doi.org/10.1021/jacs.5c01571
J. Am. Chem. Soc. 2025, 147, 17880−17889

a more in-plane orientation between the cyclopentadiene ring and COO^- than the other complex.

The nature of these noncovalent interactions was investigated by carrying out energy decomposition analysis with ALMO-EDA[42] with implicit solvent enabled. Roughly, all of the target/selector pairs followed a similar energy decomposition where the electrostatics dominate bonding (~70% of total interaction energy), with the remaining ~10% coming from polarization and ~20% from charge transfer (Table S9 and Figure S88). Among the three energy contributions, electrostatic interactions are expected to be affected the most due to the consideration of implicit solvents. For example, on the (R, R_p)−SeOxF/Boc−L−Pro pair (Figure 6e), the classical electrostatics provide 301 kJ/mol stabilization, out of which 258 kJ/mol is screened due to the presence of solvent. Using the same example pair, we tested the influence of the planar chirality on selectivity; starting from the obtained geometry, we obtained the (S, R_p)−SeOxF/Boc−L−Pro. We observed that the switch of the isobutyl group away from the carboxylate resulted in an energy increase of 0.036 eV, indicating a rather more favorable interaction in its (R, R_p) state than that in (S, R_p). Analyzing this pair's energy decomposition reveals a similar electrostatic contribution (−301 vs −299 kJ/mol for R, R_p against S, R_p), with an overall 9 kJ/mol frozen energy stabilization for the R, R_p enantiomer. This observation suggests that despite the lack of clear binding modes with the planar chiral center, long-range interactions determine the relative stability of the complexes. Overall, the DFT calculations revealed the important role of planar chirality, of which functional groups can either coordinatively or antagonistically contribute to complexation, playing a key role in enantioselective discrimination. The calculations elucidated the known [CH···O] and [CH···π] interactions, with the energetic selectivity predictions largely matching the empirical observations. EDA calculations quantified the important role of long-range electrostatics in complexations that determine the enantioselectivity.

Enantioselective Separation using Planar Chiral Polymer Electrodes. Redox-switchable chiral electrodes were fabricated by drop-casting the redox-polymer solutions onto a carbon paper strip, with the enantioselective adsorption being carried out with a medium containing racemic *N*-Boc−amino acid (Supporting Information for fabrication details). Scanning electron microscope (SEM) images with EDS mapping of key elements showed that the chiral polymers were well-distributed on carbon paper (Figure S69). Poly(R, R_p) or (S, S_p)−SeOxF were used to separate the Boc−Pro enantiomers, and poly(S, R_p)−MeOxF was evaluated for Boc−His enantiomers, following the results from the corresponding small molecules which showed the highest $|\Delta\Delta E_{1/2}|$ against each chiral selectors.

The adsorption was conducted either under an applied potential where the ferrocene moieties in the polymer can be oxidized or at open circuit potential (OCP) where the ferrocene unit remained neutral (Figure S71). An applied potential for adsorption was carefully selected to oxidize only the polymers without side reactions, such as the oxidation of the target *N*-Boc−amino acids, based on their linear sweep voltammograms (Figure S72). Under OCP, poly(R, R_p)−SeOxF adsorbed more Boc−L−Pro (7.5 mg_{Boc_L-Pro}/g_{site}) than Boc−D−Pro (3.2 mg_{Boc_D-Pro}/g_{site}) while poly(S, S_p)−SeOxF favored adsorption of Boc−D−Pro (6.2 mg_{Boc_D-Pro}/g_{site}) over Boc−L−Pro (3.8 mg_{Boc_L-Pro}/g_{site}) with the enantiomeric excess of adsorbed Boc−Pro being 43.2%ee and −21.9%ee (Figure 7a). This enantioselective preference of the SeOxF polymers observed in the adsorption agreed with the binding affinity of their corresponding small molecules (R, R_p)−SeOxF and (S, S_p)−SeOxF toward Boc−Pro enantiomers observed in the molecular recognition (Figure 6a). Under the oxidation potential of 0.34 V (vs $Ag/AgNO_3$), poly(R, R_p)−SeOxF showed increased uptake of both Boc−L and Boc−D−Pro (32.6 and 18.8 $mg_{Boc-Pro}/g_{site}$, respectively) with 26.4%ee. Lower uptake (11.5 and 10.4 $mg_{Boc-Pro}/g_{site}$) and selectivity (7.0%ee) of poly(S, S_p)−SeOxF than those of poly(R, R_p)−SeOxF was likely to be attributed to its molecular weight 1.4 times higher than that of (R, R_p), which could cause the lower utilization of the chiral binding sites. Adsorption at 0.40 V (vs $Ag/AgNO_3$) showed −1.7%ee, implying that selecting a rather moderate oxidation potential is a key to optimal uptake and enantioselectivity (Figure S77).

The release of the adsorbed Boc−Pro was conducted under a reduction potential of −0.50 V (vs $Ag/AgNO_3$) and showed up to 66−78% regeneration for both Boc−Pro enantiomers (Figure S78). The enantioselective adsorption of Boc−His using poly(S, R_p)−MeOxF under OCP and 0.35 V vs $Ag/AgNO_3$ was favorable toward Boc−D−His (25.1 and 18.5%ee, respectively) (Figure 7b) in agreement with the stronger affinity of (S, R_p)−MeOxF toward Boc−D−His (Figure 6b). The uptake at 0.35 V (vs $Ag/AgNO_3$) (41.3 mg_{Boc_D-His}/g_{site} and 25.6 mg_{Boc_L-His}/g_{site}) was similar to that under OCP (35.8 mg_{Boc_D-His}/g_{site} and 24.7 mg_{Boc_L-His}/g_{site}) because of the low electronic conductivity of the polymer film due to the disulfide cross-linking, limiting the binding sites only to the electrode surface. This low conductivity also resulted in low regeneration of Boc−His upon reduction potential (Figure S79).

A multistage adsorption cascade is proposed to achieve an enantiopure end product based on counter-current stage designs of relevance to industrial separation processes.[43,44] Poly(R, R_p)−SeOxF was evaluated for electrosorption in a solution of different fractions of Boc−Pro, and an equilibrium line was also drawn from empirical K^+s assuming the competitive Langmuir adsorption[45] (Figure 7c and Supporting Information). The Boc−L−Pro favorable adsorption by poly(R, R_p)−SeOxF was observed over the range of X_{Boc_L-Pro} between 0.1 and 0.9, in agreement with the equilibrium line. A multistage cascade, with the redox polymer as the active sorbent, consists of sets of two electrochemical cells that cycle the chiral electrode between the adsorption and desorption cell while a counter electrode is used as an electron sink/source (Figure 7d). The L-enriched solution after desorption is transferred to the next stage, while the postadsorption D-enriched solution is transferred to the previous stage in a counter-current manner. The equilibrium line suggests that from a racemic Boc−Pro mixture, 99%ee can be achieved within seven theoretical stages (Table S5). Going forward, alternative implementation formats of the redox chiral electrosorbents include electrochemically modulated chromatography mode.[46] In general, we envision that the current work provides a proof-of-concept for the applicability of the planar chiral polymers for redox-mediated chiral separation, being able to achieve electrochemically controlled performances that can lead to an enantiopure product in practical processes.

https://doi.org/10.1021/jacs.5c01571
J. Am. Chem. Soc. 2025, 147, 17880−17889

CONCLUSIONS

In this work, highly specific enantioselective interactions were achieved using redox selectors with planar chirality. The single-site binding concepts in the homogeneous phase were translated to planar chiral metallopolymers, which were then leveraged as electrosorbents for the electrochemically controlled selective adsorption and release of amino acid enantiomers. Synthesis pathways based on oxazoline chemistry were shown to lead to precise molecular control of both planar chirality and point chirality. Planar chirality was shown to be the dominant mechanism for enantioselective interactions for a range of biomolecules, with the specific strength of the interaction dependent on the functional groups inserted into the cyclopentadienyl ring. Electronic structure calculations revealed that the enantioselectivity was mainly attributed to a synergistic effect between the functional groups forming the planar chirality, as opposed to the point chirality on the oxazoline. Monomers with the planar chiral selectors were synthesized and polymerized for use as electrosorbents. Electrochemically mediated enantioselective adsorption and release were carried out, and a high enantiopurity (>99%ee) of the Boc−Pro enantiomer was achieved in a cascade electrochemical process within seven theoretical stages. These ferrocene-based planar chiral systems offer a unique platform for electrochemically controlled enantioselective separations. In the long term, we envision next-generation molecular innovations on this concept, coupled with electrochemical systems design, to be deployable as practical separation platforms for API and biomolecular purification.

ASSOCIATED CONTENT

Supporting Information

The Supporting Information is available free of charge at https://pubs.acs.org/doi/10.1021/jacs.5c01571.

Additional experimental details and supporting data including: synthesis protocols for redox molecules, monomers, and polymers; electrode fabrication procedures; chemical characterization of small molecules and polymers; analytics of small molecules in solution; materials characterization including circular dichroism and SEM; methods for enatioselective recognition and electrochemical separations; computational methods for electronic structure calculations and analysis of data (PDF)

AUTHOR INFORMATION

Corresponding Authors

Fabio Zazyki Galetto − *Department of Chemistry, Universidade Federal de Santa Catarina, Florianópolis, Santa Catarina CEP 88035-972, Brazil*; Email: galetto.f.z@ufsc.br

Xiao Su − *Department of Chemical and Biomolecular Engineering, University of Illinois Urbana−Champaign, Urbana, Illinois 61801, United States; Department of Chemistry, University of Illinois Urbana−Champaign, Urbana, Illinois 61801, United States;* orcid.org/0000-0001-7794-290X; Email: x2su@illinois.edu

Authors

Jemin Jeon − *Department of Chemical and Biomolecular Engineering, University of Illinois Urbana−Champaign, Urbana, Illinois 61801, United States*

Yuri Giovane Kappenberg − *Department of Chemical and Biomolecular Engineering, University of Illinois Urbana−Champaign, Urbana, Illinois 61801, United States*

Ankit Kumar Gautam − *Department of Chemical and Biomolecular Engineering, University of Illinois Urbana−Champaign, Urbana, Illinois 61801, United States*

Ching-Yu Chen − *Department of Chemical and Biomolecular Engineering, University of Illinois Urbana−Champaign, Urbana, Illinois 61801, United States*

Johannes Elbert − *Department of Chemical and Biomolecular Engineering, University of Illinois Urbana−Champaign, Urbana, Illinois 61801, United States;* orcid.org/0000-0002-7682-8686

Alexander V. Mironenko − *Department of Chemical and Biomolecular Engineering, University of Illinois Urbana−Champaign, Urbana, Illinois 61801, United States;* orcid.org/0000-0001-7490-5038

Complete contact information is available at: https://pubs.acs.org/10.1021/jacs.5c01571

Author Contributions

[‖]J.J. and Y.G.K. have equally contributed to the work.

Notes

The authors declare no competing financial interest.

ACKNOWLEDGMENTS

This material is based upon work supported by the National Science Foundation under CBET Grant #1942971 (recipient: X.S.). F.Z.G. was partially supported by the Conselho Nacional de Desenvolvimento Científico e Tecnológico (CNPq) Grant 457479/2014-0. J. J. would like to thank Prof. Scott Denmark for access to the ORD instrumentation and Shoya Takeda for helping with experiments on electrochemical characterization. The authors acknowledge the use of the instrumentation at NMR Lab, George L. Clark X-ray Facility, and Microanalysis Laboratory in the School of Chemical Sciences (SCS).

REFERENCES

(1) Xue, L.; Thatte, A. S.; Mai, D.; Haley, R. M.; Gong, N.; Han, X.; Wang, K.; Sheppard, N. C.; June, C. H.; Mitchell, M. J. Responsive biomaterials: optimizing control of cancer immunotherapy. *Nat. Rev. Mater.* **2024**, *9* (2), 100−118.

(2) Xia, X.; Spadaccini, C. M.; Greer, J. R. Responsive materials architected in space and time. *Nat. Rev. Mater.* **2022**, *7* (9), 683−701.

(3) Srimuk, P.; Su, X.; Yoon, J.; Aurbach, D.; Presser, V. Charge-transfer materials for electrochemical water desalination, ion separation and the recovery of elements. *Nat. Rev. Mater.* **2020**, *5* (7), 517−538.

(4) Langton, M. J. Engineering of stimuli-responsive lipid-bilayer membranes using supramolecular systems. *Nat. Rev. Chem.* **2021**, *5* (1), 46−61.

(5) Fukino, T.; Yamagishi, H.; Aida, T. Redox-Responsive Molecular Systems and Materials. *Adv. Mater.* **2017**, *29* (25), No. 1603888.

(6) Shang, X.; Song, I.; Jung, G. Y.; Choi, W.; Ohtsu, H.; Lee, J. H.; Koo, J. Y.; Liu, B.; Ahn, J.; Kawano, M.; Kwak, S. K.; Oh, J. H. Chiral self-sorted multifunctional supramolecular biocoordination polymers and their applications in sensors. *Nat. Commun.* **2018**, *9* (1), No. 3933.

(7) Formen, J. S. S. K.; Wolf, C. Chiroptical Switching and Quantitative Chirality Sensing with (Pseudo) halogenated Quinones. *Angew. Chem.* **2021**, *133* (52), 27237−27244.

(8) Torsi, L.; Farinola, G. M.; Marinelli, F.; Tanese, M. C.; Omar, O. H.; Valli, L.; Babudri, F.; Palmisano, F.; Zambonin, P. G.; Naso, F. A

sensitivity-enhanced field-effect chiral sensor. *Nat. Mater.* **2008**, *7* (5), 412−417.
(9) Mirri, G.; Bull, S. D.; Horton, P. N.; James, T. D.; Male, L.; Tucker, J. H. Electrochemical method for the determination of enantiomeric excess of binol using redox-active boronic acids as chiral sensors. *J. Am. Chem. Soc.* **2010**, *132* (26), 8903−8905.
(10) Su, X.; Kulik, H. J.; Jamison, T. F.; Hatton, T. A. Anion-Selective Redox Electrodes: Electrochemically Mediated Separation with Heterogeneous Organometallic Interfaces. *Adv. Funct. Mater.* **2016**, *26* (20), 3394−3404.
(11) Chen, R.; Feng, J.; Jeon, J.; Sheehan, T.; Rüttiger, C.; Gallei, M.; Shukla, D.; Su, X. Structure and Potential-Dependent Selectivity in Redox-Metallopolymers: Electrochemically Mediated Multicomponent Metal Separations. *Adv. Funct. Mater.* **2021**, *31* (15), No. 2009307.
(12) Cotty, S.; Jeon, J.; Elbert, J.; Jeyaraj, V. S.; Mironenko, A. V.; Su, X. Electrochemical recycling of homogeneous catalysts. *Sci. Adv.***2022**. *8* 42 eade3094.
(13) Chung, C.-H.; Cotty, S.; Jeon, J.; Elbert, J.; Su, X. Auto-oxidation of redox electrodes for the selective recovery of platinum group metals. *J. Mater. Chem. A* **2024**, *12* (25), 15006−15018.
(14) Cotty, S. R.; Faniyan, A.; Elbert, J.; Su, X. Redox-mediated electrochemical liquid−liquid extraction for selective metal recovery. *Nat. Chem. Eng.* **2024**, *1* (4), 281−292.
(15) López, R.; Palomo, C. Planar Chirality: A Mine for Catalysis and Structure Discovery. *Angew. Chem., Int. Ed.* **2022**, *61* (13), No. e202113504.
(16) Gulder, T.; Baran, P. S. Strained cyclophane natural products: Macrocyclization at its limits. *Nat. Prod. Rep.* **2012**, *29* (8), 899−934.
(17) Hassan, Z.; Spuling, E.; Knoll, D. M.; Lahann, J.; Bräse, S. Planar chiral [2.2] paracyclophanes: from synthetic curiosity to applications in asymmetric synthesis and materials. *Chem. Soc. Rev.* **2018**, *47* (18), 6947−6963.
(18) Zhou, L.; Cheng, H.-G.; Li, L.; Wu, K.; Hou, J.; Jiao, C.; Deng, S.; Liu, Z.; Yu, J.-Q.; Zhou, Q. Synthesis of planar chiral ferrocenes via enantioselective remote C−H activation. *Nat. Chem.* **2023**, *15* (6), 815−823.
(19) Agranat, I.; Wainschtein, S. R.; Zusman, E. Z. The predicated demise of racemic new molecular entities is an exaggeration. *Nat. Rev. Drug Discovery* **2012**, *11* (12), 972−973.
(20) McVicker, R. U.; O'Boyle, N. M. Chirality of New Drug Approvals (2013−2022): Trends and Perspectives. *J. Med. Chem.* **2024**, *67* (4), 2305−2320.
(21) Okamoto, Y.; Ikai, T. Chiral HPLC for efficient resolution of enantiomers. *Chem. Soc. Rev.* **2008**, *37* (12), 2593−2608.
(22) Speybrouck, D.; Lipka, E. Productivity and solvent waste in supercritical fluid chromatography for preparative chiral separations: a guide for a convenient strategy. *J. Chromatogr. A* **2020**, *1610*, No. 460549.
(23) Sheldon, R. A. The E factor 25 years on: the rise of green chemistry and sustainability. *Green Chem.* **2017**, *19* (1), 18−43.
(24) Rajendran, A.; Paredes, G.; Mazzotti, M. Simulated moving bed chromatography for the separation of enantiomers. *J. Chromatogr. A* **2009**, *1216* (4), 709−738.
(25) Candeago, R.; Wang, H.; Nguyen, M.-T.; Doucet, M.; Glezakou, V.-A.; Browning, J. F.; Su, X. Unraveling the Role of Solvation and Ion Valency on Redox-Mediated Electrosorption through In Situ Neutron Reflectometry and Ab Initio Molecular Dynamics. *JACS Au* **2024**, *4* (3), 919−929.
(26) Jeon, J.; Chung, C.-H.; Roh, S.; Bergman, E.; Wang, M.; Su, X. Olefin-Assisted Electrochemical Recycling of Homogeneous Hydrosilylation Catalysts in Nonpolar Media. *JACS Au* **2025**, *5* (3), 1221−1231.
(27) Kim, N.; Jeyaraj, V. S.; Elbert, J.; Seo, S. J.; Mironenko, A. V.; Su, X. Redox-Responsive Halogen Bonding as a Highly Selective Interaction for Electrochemical Separations. *JACS Au* **2024**, *4* (7), 2523−2538.
(28) Niu, X.; Mo, Z.; Yang, X.; Shuai, C.; Liu, N.; Guo, R. Graphene-ferrocene functionalized cyclodextrin composite with high electrochemical recognition capability for phenylalanine enantiomers. *Bioelectrochemistry* **2019**, *128*, 74−82.
(29) Wu, D.; Ma, C.; Pan, F.; Tao, Y.; Kong, Y. Strategies to Achieve a Ferrocene-Based Polymer with Reversible Redox Activity for Chiral Electroanalysis of Nonelectroactive Amino Acids. *Anal. Chem.* **2021**, *93* (29), 10160−10166.
(30) Tarrío, F. R.; Quiñoá, E.; Fernández, G.; Freire, F. Multi-chiral materials comprising metallosupramolecular and covalent helical polymers containing five axial motifs within a helix. *Nat. Commun.* **2023**, *14* (1), No. 3348.
(31) Dai, H.; Hong, R.; Ma, Y.; Cheng, X.; Zhang, W. A Subtle Change in the Flexible Achiral Spacer Does Matter in Supramolecular Chirality: Two-Fold Odd-Even Effect in Polymer Assemblies. *Angew. Chem., Int. Ed.* **2023**, *62* (50), No. e202314848.
(32) Li, G.; Xu, M.; Zhang, S.; Yang, G.; Li, W. Reversible Controlling the Supramolecular Chirality of Side Chain Azobenzene Polymers: Chiral Induction and Modulation. *Macromol. Rapid Commun.* **2022**, *43* (6), No. 2100904.
(33) Martin, V.; Egelund, P. H. G.; Johansson, H.; Le Quement, S. T.; Wojcik, F.; Pedersen, D. S. Greening the synthesis of peptide therapeutics: an industrial perspective. *RSC Adv.* **2020**, *10* (69), 42457−42492.
(34) Jeon, J.; Elbert, J.; Chung, C.-H.; Chae, J.; Su, X. Chiral Metallopolymers for Redox-Mediated Enantioselective Interactions. *Adv. Funct. Mater.* **2023**, *33* (27), No. 2301545.
(35) Herbert, S. A.; Castell, D. C.; Clayden, J.; Arnott, G. E. Manipulating the Diastereoselectivity of Ortholithiation in Planar Chiral Ferrocenes. *Org. Lett.* **2013**, *15* (13), 3334−3337.
(36) Peluso, P.; Mamane, V. Ferrocene derivatives with planar chirality and their enantioseparation by liquid-phase techniques. *Electrophoresis* **2023**, *44* (1−2), 158−189.
(37) Jain, V. K. An Overview of Organoselenium Chemistry: From Fundamentals to Synthesis. In *Organoselenium Compounds in Biology and Medicine: Synthesis, Biological and Therapeutic Treatments*; Jain, V. K.; Priyadarsini, K. I., Eds.; The Royal Society of Chemistry, 2017.
(38) Teixidor, F.; Barberà, G.; Vaca, A.; Kivekäs, R.; Sillanpää, R.; Oliva, J.; Viñas, C. Are Methyl Groups Electron-Donating or Electron-Withdrawing in Boron Clusters? Permethylation of o-Carborane. *J. Am. Chem. Soc.* **2005**, *127* (29), 10158−10159.
(39) Hein, R.; Docker, A.; Davis, J. J.; Beer, P. D. Redox-Switchable Chalcogen Bonding for Anion Recognition and Sensing. *J. Am. Chem. Soc.* **2022**, *144* (19), 8827−8836.
(40) Steed, J. W.; Atwood, J. L. *Supramolecular Chemistry*; John Wiley & Sons, 2022.
(41) Okamoto, Y. Precision synthesis, structure and function of helical polymers. *Proc. Jpn. Acad., Ser. B* **2015**, *91* (6), 246−261.
(42) Khaliullin, R. Z.; Cobar, E. A.; Lochan, R. C.; Bell, A. T.; Head-Gordon, M. Unravelling the Origin of Intermolecular Interactions Using Absolutely Localized Molecular Orbitals. *J. Phys. Chem. A* **2007**, *111* (36), 8753−8765.
(43) Yilmaz-Turan, S.; Jiménez-Quero, A.; Moriana, R.; Arte, E.; Katina, K.; Vilaplana, F. Cascade extraction of proteins and feruloylated arabinoxylans from wheat bran. *Food Chem.* **2020**, *333*, No. 127491.
(44) Patil, N. V.; Janssen, A. E. M.; Boom, R. M. The potential impact of membrane cascading on downstream processing of oligosaccharides. *Chem. Eng. Sci.* **2014**, *106*, 86−98.
(45) Masel, R. I. *Principles of Adsorption and Reaction on Solid Surfaces*.; John Wiley & Sons, 1996; Vol. *3*.
(46) Harnisch, J. A.; Porter, M. D. Electrochemically modulated liquid chromatography: an electrochemical strategy for manipulating chromatographic retention. *Analyst* **2001**, *126* (11), 1841−1849.

https://doi.org/10.1021/jacs.5c01571
J. Am. Chem. Soc. 2025, 147, 17880−17889